CHEMISTRY & SUSTAINABILITY

CHEMSUSCHEM

ENERGY & MATERIALS

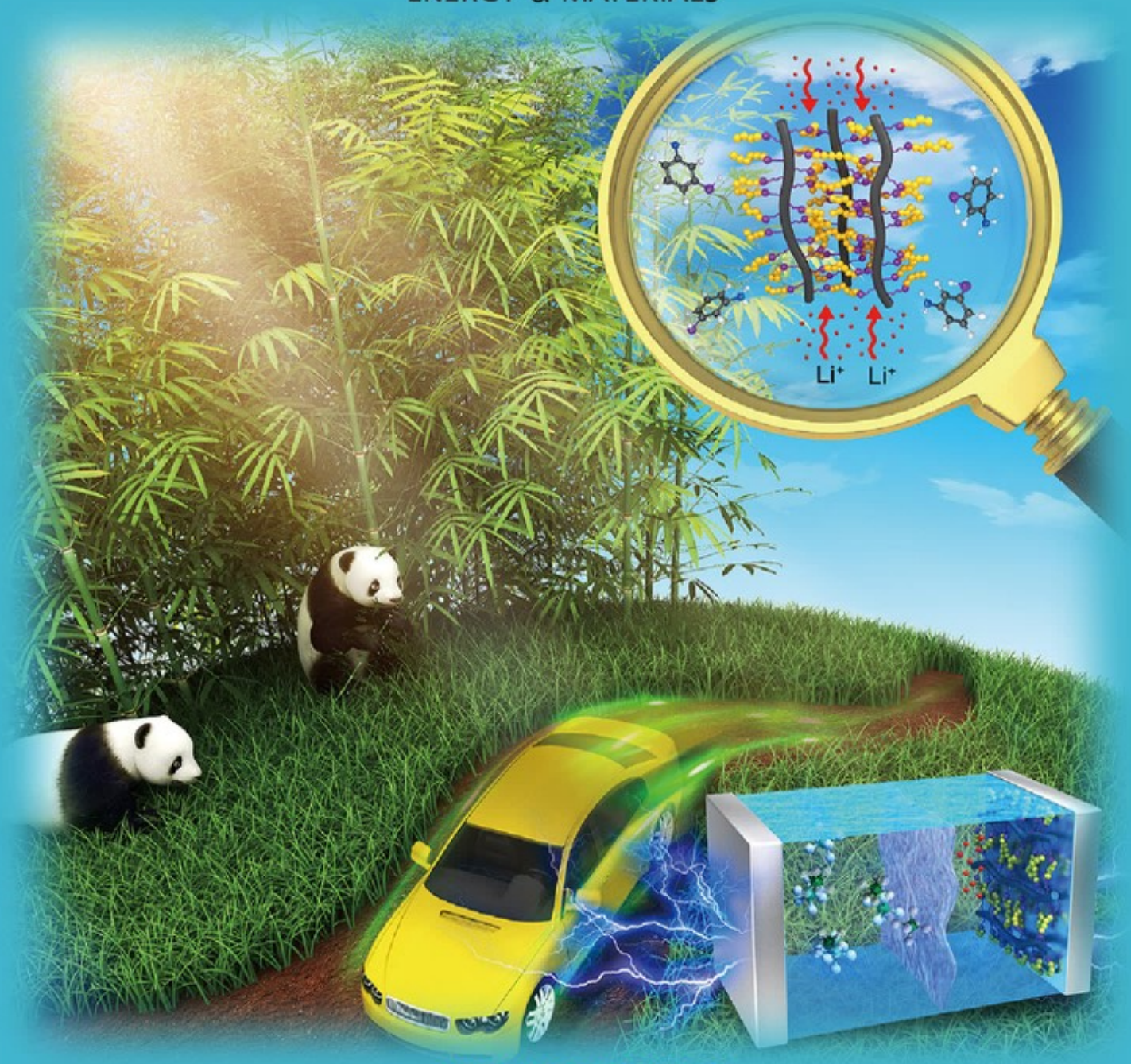

17/2017

Cover Feature:

Zeng et al.

Conducting Polymers Crosslinked with Sulfur as Cathode Materials for High-Rate, Ultralong-Life Lithium–Sulfur Batteries

A Journal of

ChemPubSoc Europe

WILEY-VCH

www.chemsuschem.org

ChemPubSoc Europe

DOI: 10.1002/cssc.201700913

CHEMSUSCHEM Full Papers

Conducting Polymers Crosslinked with Sulfur as Cathode Materials for High-Rate, Ultralong-Life Lithium–Sulfur Batteries

Shuaibo Zeng,[a] Ligui Li,*[a, b] Lihong Xie,[a] Dengke Zhao,[a] Nan Wang,[a] and Shaowei Chen*[a, c]

Low electrical conductivity and a lack of chemical confinement are two major factors that limit the rate performances and cycling stabilities of cathode materials in lithium–sulfur (Li–S) batteries. Herein, sulfur is copolymerized with poly(*m*-aminothiophenol) (PMAT) nanoplates through inverse vulcanization to form the highly crosslinked copolymer cp(S-PMAT) in which approximately 80 wt% of the feed sulfur is bonded chemically to the thiol groups of PMAT. A cp(S-PMAT)/C-based cathode exhibits a high discharge capacity of 1240 mAh g^{-1} at 0.1 C and remarkable rate capacities of 880 mAh g^{-1} at 1 C and 600 mAh g^{-1} at 5 C. Moreover, it can retain a capacity of 495 mAh g^{-1} after 1000 deep discharge–charge cycles at 2 C; this corresponds to a retention of 66.9% and a decay rate of only 0.040% per cycle. Such a remarkable rate performance is attributed to the highly conductive pathways of PMAT nanoplates, and the excellent cycling stability is ascribed mainly to the chemical confinement of sulfur through a large number of stable covalent bonds between sulfur and the thiol groups of PMAT. The results suggest that this strategy is a viable paradigm for the design and engineering of conducting polymers with reactive functional groups as effective electrode materials for high-performance Li–S batteries.

Introduction

Li–S batteries have attracted extensive research interest as promising electrochemical energy-conversion and storage devices largely because of their high theoretical capacity (1672 mAh g^{-1}), ecofriendliness, and low operation costs as well as the earth-abundance of sulfur.[1,2] However, as several critical challenges remain with the cathodes of Li–S batteries, their widespread commercialization is limited severely. For example, during the cycling process, lithium polysulfide intermediates such as Li_2S_x ($x = 4$ to 8) dissolve readily into ether-based electrolytes, and this causes the loss of active sulfur from the cathode and the emergence of the shuttle effect, which leads to reduced capacity and safety issues.[3] In addition, the insulating nature of sulfur and lithium sulfide (5×10^{-30} S cm^{-1}) compromises the sulfur utilization and rate performance of the battery.[4] The large volume expansion (≈80%) for sulfur lithiation also deteriorates the contact between the physically adsorbed sulfur domains and the underlying current collectors and causes rapid degradation in device performance.[5,6] To mitigate these issues, sulfur is generally embedded in polymers,[2,5,7] metal–organic frameworks,[8] and carbon-based materials[9] or physical hybrids are formed with well-defined (core–shell,[10] yolk–shell,[11] layer,[12,13] and sandwich-type)[13,14] nanostructures, which enhance the electrical conductivity of the cathode substantially and impede the loss of active sulfur.[15] However, the inert surfaces of these electrode materials make it difficult to form sufficient chemical bonds with the supporting sulfur to produce potent confinement knots, and the large volume fluctuations for the repetitive lithiation/dethiation of sulfur/lithium sulfides inevitably causes the detachment of active materials from the current collectors and, hence, capacity degradation.[16]

Owing to these limitations of the physical-confinement strategies, the development of effective strategies based on chemical confinement is highly desired. To this end, the copolymerization of sulfur with polymerizable monomers[17] or polymers with reactive groups[18] through thermally activated radical polymerization has been studied extensively. However, sulfur-rich copolymers are mostly insulating or of low conductivity, which restricts the loading of active sulfur to only 1.0 mg cm^{-2} or lower (Table S1 in the Supporting Information); hence, these strategies are not beneficial for rate-capacity improvement.[2,19] Therefore, the direct copolymerization of sulfur with highly conductive polymers or blocks represents a judicious way to

[a] S. Zeng, Prof. L. Li, L. Xie, D. Zhao, N. Wang, Prof. S. Chen
Guangzhou Key Laboratory for Surface Chemistry of Energy Materials
New Energy Research Institute, College of Environment and Energy
South China University of Technology
Guangzhou Higher Education Mega Center
Guangzhou 510006 (P. R. China)
E-mail: esguili@scut.edu.cn

[b] Prof. L. Li
Guangdong Provincial Key Laboratory of Atmospheric Environment and Pollution Control
College of Environment and Energy
South China University of Technology
Guangzhou 510006 (P. R. China)

[c] Prof. S. Chen
Department of Chemistry and Biochemistry, University of California
1156 High Street, Santa Cruz, CA 95064 (USA)
E-mail: shaowei@ucsc.edu

Supporting Information for this article can be found under: https://doi.org/10.1002/cssc.201700913.

overcome the current predicament. This is the primary motivation of the present work.

In this work, *m*-aminothiophenol was homopolymerized to form the conducting polymer poly(*m*-aminothiophenol) (PMAT) with abundant thiol groups, which were used for postsynthesis copolymerization with elemental sulfur through inverse vulcanization to form cp(S-PMAT). The utilization of cp(S-PMAT) as a cathode material resulted in a remarkable enhancement of the rate performance and stability of Li–S batteries at a much higher active sulfur loading of 1.5 mg cm^{-2}, and the devices exhibited reversible capacities of 1240 mAh g^{-1} at 0.1 C, 880 mAh g^{-1} at 1 C, and 600 mAh g^{-1} at 5 C as well as a discharge capacity of 495 mAh g^{-1} even after 1000 deep charge–discharge cycles at 2 C; this represents a capacity retention of 66.9% and a low capacity-fading rate of only 0.040% per cycle. The superb performance of the cp(S-PMAT) cathode is attributed to the highly stable crosslinked nanostructures, which contain approximately 80 wt% of crosslinked sulfur and can retain half of their initial value after 1000 deep charge–discharge cycles at 2 C.

Results and Discussion

The synthetic strategy is illustrated in Figure 1 a; 3-aminothiophenol was first dissolved in an aqueous HCl solution, and the addition of an aqueous solution of ammonium persulfate (APS) initiated the polymerization of 3-aminothiophenol to form PMAT, which consists of a conducting polyaniline backbone with thiol side groups. Note that PMAT is stable below 200 °C, as evidenced by the negligible weight loss in thermogravimetric analysis (TGA) measurements (Figure S1 a). The ring-opening radical polymerization of elemental sulfur with the thiol groups of PMAT was performed at 170 °C to produce the cp(S-PMAT) copolymer with the sulfur side chains as intermolecular crosslinkers. Such sulfur side chains can be broken into Li_2S during discharge, whereas the reversible assembly of S^{2-} ions into the long sulfur side chains between the PMAT molecular chains occurs in the charging state (Figure 1 b), similarly to the processes in previously reported sulfur-rich copolymers.[17a,f, 20] Such a copolymer not only provides continuous pathways for electron transport but also suppresses the diffusion of polysulfides owing to the chemical bonds between the thiol groups of the conducting polymer and sulfur; hence, it can be used as an electroactive material to enhance the rate performance and cycling stability of cathodes in Li–S batteries (Figure 1 c).

The morphologies and structures of the materials were first examined by SEM and TEM measurements. A representative SEM image of sulfur powder is shown in Figure 2 a, and isolated nanoparticles with diameters ranging from tens to hundreds of nanometers are observed. For the PMAT sample (Figure 2 b–c), a large number of interconnected triangular nanosheets with thicknesses of 50 to 100 nm are observed. After PMAT is physically mixed with sulfur, micrometer-scale particles and pinholes can be seen in the resulting S&PMAT sample (Figure 2 d). In sharp contrast, if sulfur is copolymerized with PMAT (Figure 2 e), the particle size is reduced dramatically, and a

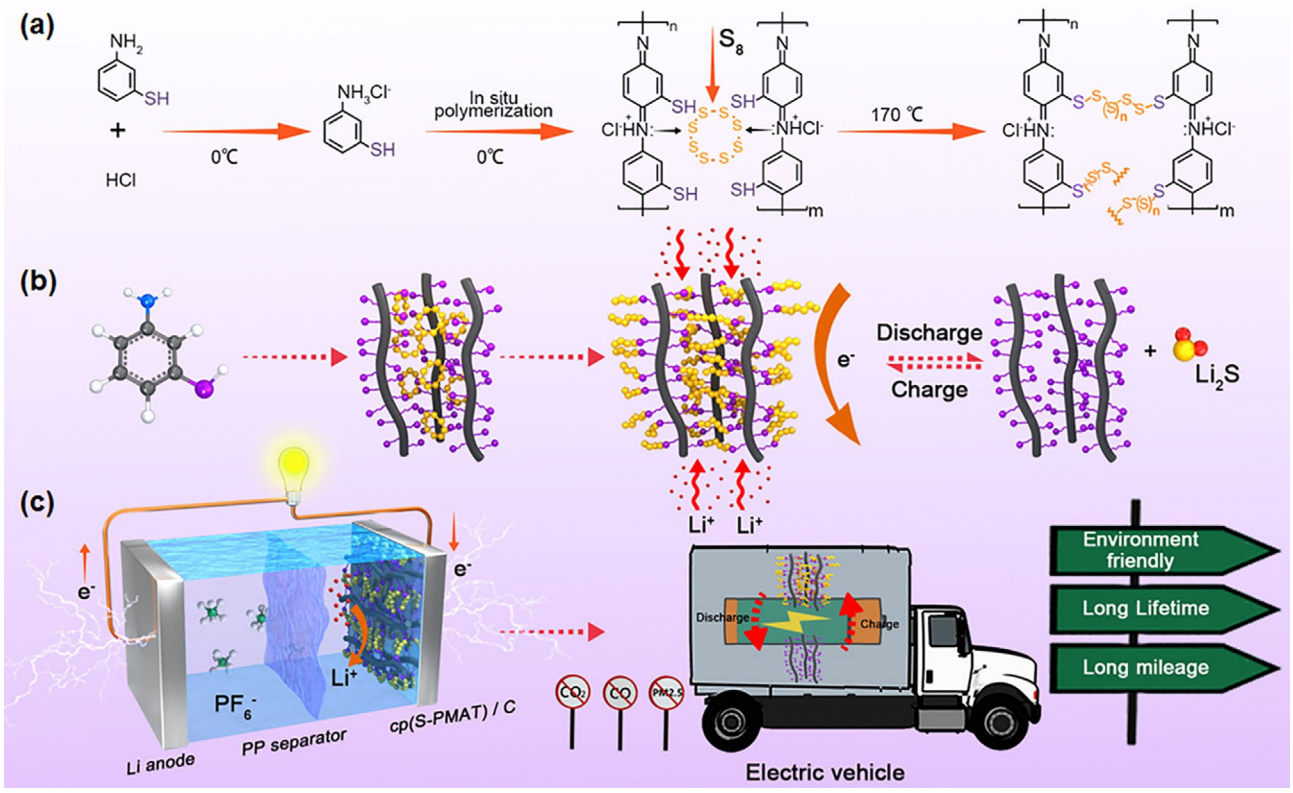

Figure 1. (a) The synthesis of the cp(S-PMAT) copolymer. (b) The structural evolution in the synthesis of cp(S-PMAT) and discharge–charge process. (c) The device configuration of a Li–S battery with cp(S-PMAT) as the cathode material.

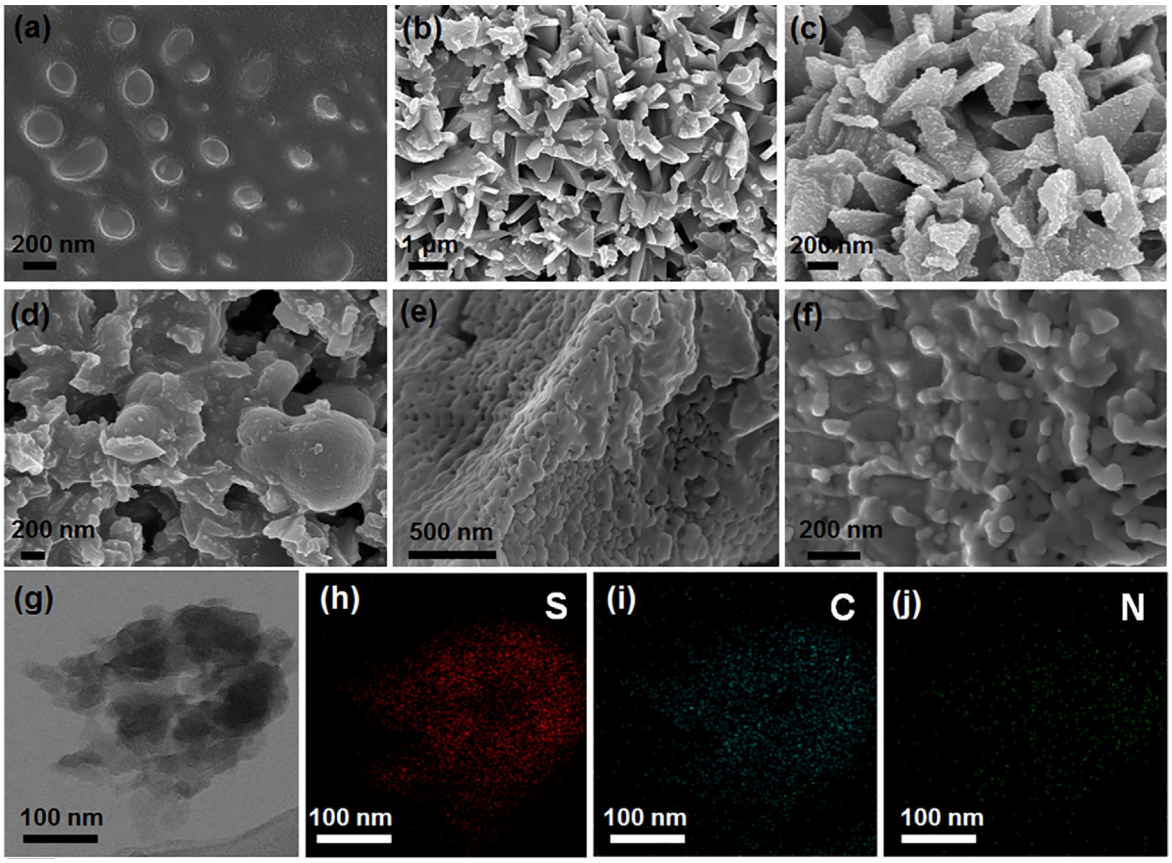

Figure 2. SEM images of (a) sulfur, (b, c) PMAT, (d) S&PMAT, and (e, f) cp(S-PMAT). (g) TEM image of cp(S-PMAT) and the corresponding elemental maps for (h) S, (i) C, and (j) N.

large number of smaller pinholes form with diameters in the rage 10 to 100 nm. In the higher magnification SEM image (Figure 2 f), homogeneous interconnected nanoparticles of approximately 50 nm diameter can be observed on the surfaces of cp(S-PMAT), which are smoother than those of S&PMAT (Figure 2 d). The corresponding TEM images in Figures 2 g and S2 reveal that cp(S-PMAT) indeed consists of many closely packed nanoparticles; cp(S-PMAT) is not a physical mixture of sulfur and PMAT but a chemically bonded copolymer, as evidenced by the homogeneous distributions of S, C, and N over the entire sample surface (Figure 2 h–j). Note that the large numbers of small pinholes and interconnected nanoparticles are beneficial to maximize the contact with the electrolyte and facilitate the diffusion of lithium ions (vide infra). Differential scanning calorimetry (DSC) analysis was performed to confirm further the formation of covalent crosslinks between S_8 and PMAT. As depicted in Figure S1 b, elementary sulfur showed four apparent endothermic peaks in the heating curve; the first one at approximately 110 °C is attributed to the solid–solid phase transition from an orthorhombic form to a monoclinic one, the second one at approximately 130 °C is ascribed to the solid–liquid phase transition (i.e., melting), and the third one at approximately 178 °C results from the ring-opening of S_8 to form biradicals. The fourth one at approximately 310 °C is significantly wider than the other three, probably because of the combined contributions of the evaporation and boiling of sulfur liquid, in accord with the abrupt weight loss within this temperature range in the TGA diagram for elementary sulfur (Figure S1 a). For the cp(S-PMAT) and S&PMAT samples, the first two endothermic peaks were also identified at approximately 110 and 130 °C, but no peaks were observed at approximately 178 °C, as indicated by the light-blue dashed ellipse in Figure S1 b. This phenomenon suggests that the ring-opening of S_8 occurs to form covalent bonds with the thiol groups on PMAT.

Energy-dispersive X-ray spectroscopy (EDS) measurements (Figure 3 a) show that cp(S-PMAT) comprises only C, O, N, and S with contents of 16.15 wt% for C, 0.51 wt% for O, 2.36 wt% for N, and 80.98 wt% for S. The X-ray photoelectron spectroscopy (XPS) survey spectrum of cp(S-PMAT) is depicted in Figure 3 b, and the N 1s, C 1s, S 2s, and S 2p electrons can be identified clearly at binding energies (BEs) of 400.1, 284.0, 226.7, and 163.2 eV, respectively. Note that the binding energy of the S 2p electrons for cp(S-PMAT) shows a negative shift of 0.23 eV compared with that of elemental sulfur (Figure 3 c), and this is indicative of weakened S–S bonds after the ring-opening polymerization of S_8 with PMAT. Such a characteristic may improve the lithiation kinetics at the cp(S-PMAT) cathode.[21] The formation of crosslinked cp(S-PMAT) was evidenced by the color change of PMAT from grey-yellow to dark grey (Figure S3). Furthermore, after cp(S-PMAT) was soaked in CS_2 to remove uncrosslinked sulfur, the XPS measurements showed that the

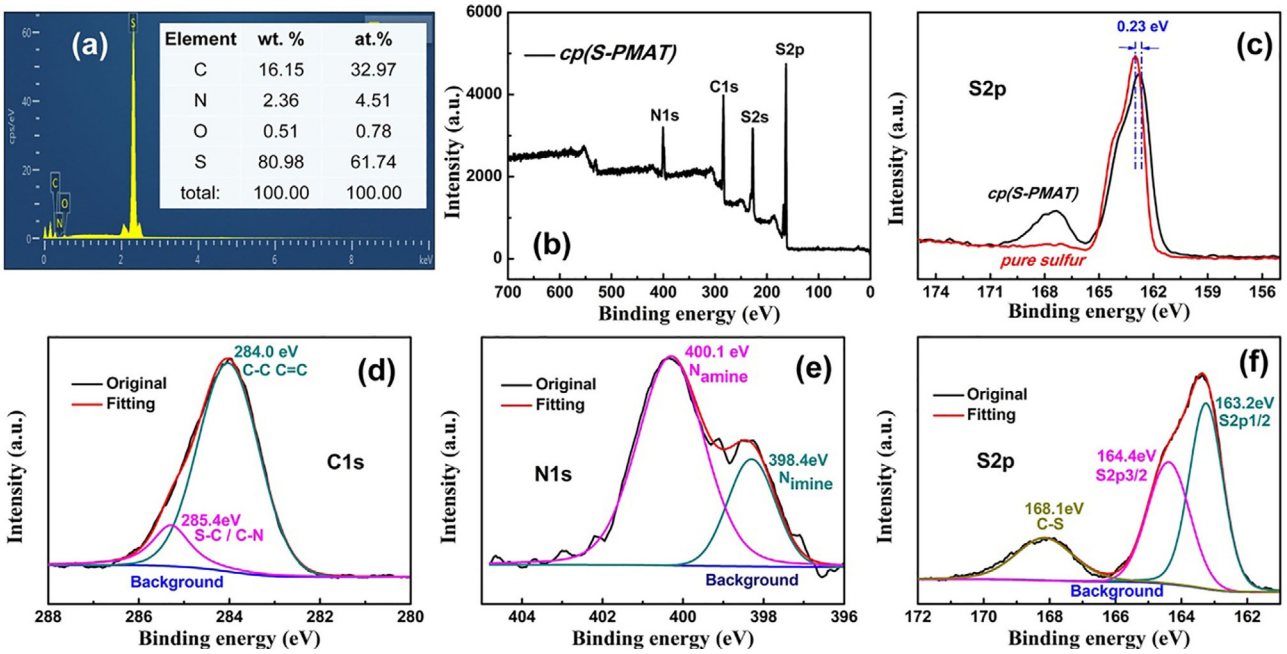

Figure 3. (a) EDS spectrum of cp(S-PMAT); the inset is a summary of the elemental contents in the sample. (b) XPS survey spectrum of cp(S-PMAT). (c) High-resolution S 2p spectra of cp(S-PMAT) and elemental sulfur. High-resolution (d) C 1s, (e) N 1s, and (f) S 2p spectra of cp(S-PMAT). The black curves are the experimental data, and the colored curves are deconvolution fits.

ratios of the integrated peak areas of S 2s versus C 1s and S 2p versus C 1s were only slightly lower than those in the untreated cp(S-PMAT) (Figure S4 a). Calculations from the XPS results suggest that approximately 83.3 wt% of the sulfur feed was converted to crosslinked sulfur in cp(S-PMAT) through the formation of covalent bonds with the thiol groups of PMAT. Consistent results were obtained through UV/Vis absorption spectroscopy (Figure S5). Interestingly, the XRD pattern of cp(S-PMAT) resembles that of elemental sulfur (Figure S6) and remained virtually unchanged after the CS_2 wash except for a small intensity decrease. These observations suggest that the sulfur in cp(S-PMAT) remained crystalline after the crosslinking process.

For the high-resolution C 1s XPS scan (Figure 3 d), deconvolution yielded two pairs of peaks located at BE = 285.4 and 284.0 eV, which may be ascribed to C–S/C–N and C–C/C=C bonds,[22] respectively. The formation of C–S/C–N bonds in cp(S-PMAT) indicates that the thiol groups were retained during the oxidation polymerization process. The deconvolution of the high-resolution N 1s spectrum yielded two peaks at BE = 398.4 and 400.1 eV (Figure 3 e), which correspond to imine-type and amine-type N atoms, respectively.[23] Note that polyaniline can reach its conductive state through the protonation of the imine-type N atoms or the oxidation of the amine-type N atoms in the fully reduced leucoemeraldine state.[24] As oxidation polymerization was used for the synthesis of PMAT in a diluted aqueous solution of HCl, it was anticipated that the PMAT in the present work would be highly conductive (vide infra).

Similarly, the high-resolution S 2p scan of cp(S-PMAT) can be deconvoluted into three peaks at the BE = 163.2, 164.4 and 168.1 eV (Figure 3 f), which are ascribed to S $2p_{1/2}$, S $2p_{3/2}$, and S–C, respectively.[25] Again, the formation of S–C bonds in cp(S-PMAT) signifies the retention of thiol groups in PMAT after the oxidation polymerization

The performance of cp(S-PMAT) as a cathode material for Li–S batteries was then examined in a coin-type prototype (Figure 4 a). The electrical conductivity was first evaluated through two-probe measurements. The electrical conductivity for elemental sulfur alone (S/C) was estimated to be 4.35×10^{-7} S cm^{-1} (Figure 4 b); however, after the addition of highly conductive PMAT with an electrical conductivity of 0.12 S cm^{-1} (Figure S7), the electrical conductivity of the resulting physical mixture (S&PMAT/C) increased by approximately two orders of magnitude to 9.81×10^{-5} S cm^{-1}. For cp(S-PMAT)/C with the sulfur crosslinked covalently to PMAT, the electrical conductivity increased further to 1.92×10^{-3} S cm^{-1} (all at the same S loading). That is, the incorporation of the conducting polymer PMAT into S, in particular, the formation of a covalently crosslinked copolymer, led to a marked enhancement of the electrical conductivity.

Consistent results were obtained through electrochemical impedance spectroscopy (EIS) measurements. From the Nyquist plots depicted in Figure 4 c, one can see that all three samples show a semicircle in the high-frequency region along with a radial oblique line in the low-frequency region. The former is associated with the charge-transfer resistance (R_{ct}),[23] which was 202.3 Ω for S/C but only 98.3 Ω for S&PMAT and even lower at 48.7 Ω for cp(S-PMAT)/C. For the radial oblique lines in the low-frequency region, the decrease of the slope in the order S/C > S&PMAT > cp(S-PMAT) suggests diminishing resistance from ion diffusion within the electrode. These results

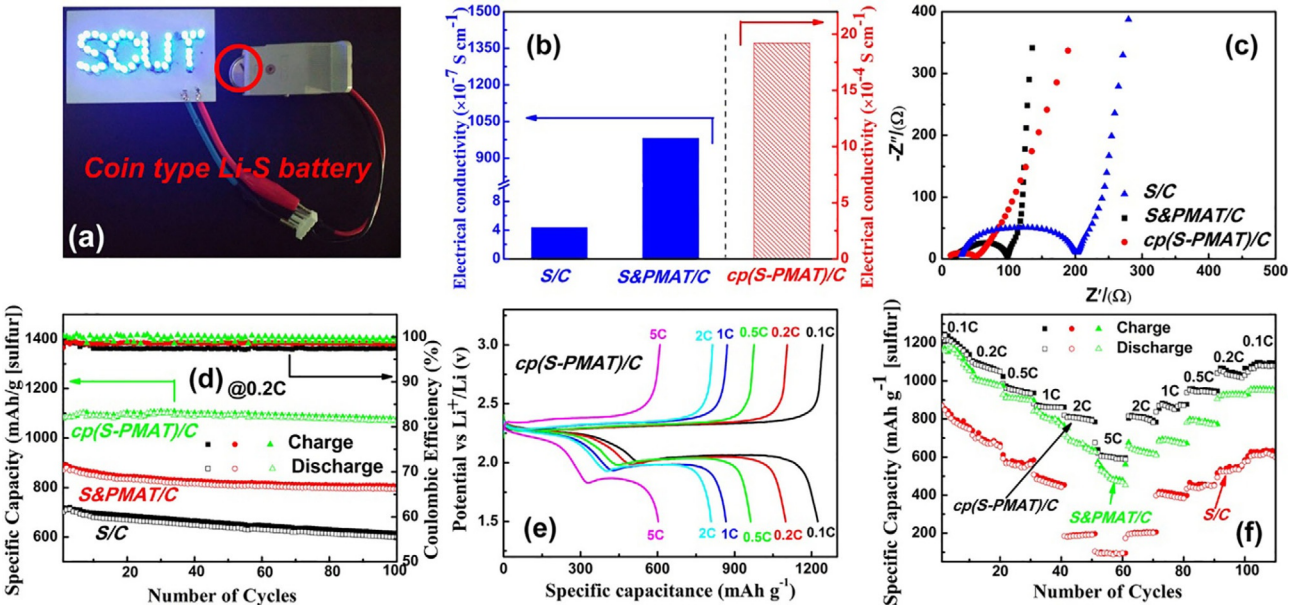

Figure 4. (a) LEDs lit by a coin-type Li–S battery with a cp(S-PMAT)/C cathode. (b) Electrical conductivities of S/C, S&PMAT/C, and cp(S-PMAT)/C cathodes. (c) EIS spectra of S/C, S&PMAT/C, and cp(S-PMAT)/C cathodes. (d) Cycling performances and coulombic efficiencies of different cathodes at 0.2 C. (e) Typical voltage profiles of the cp(S-PMAT)/C cathode at various rates. (f) Rate capacity of the cp(S-PMAT)/C cathode at varied current densities.

indicate that both the electron-transfer and the ion-transfer dynamics were enhanced markedly by the copolymerization of sulfur with PMAT to form a highly crosslinked copolymer.

The cycling stabilities of the Li–S batteries with the various cathode materials at an active sulfur loading of 1.5 mg cm^{-2} (Figure 4 d) are much higher than those of the leading sulfur-rich polymer cathodes reported recently (Table S1). The cp(S-PMAT)/C cathode exhibited a specific capacity of 1085 mAh g^{-1} at 0.2 C (1 C = 1672 mA g^{-1}), which is much higher than those for S&PMAT/C (892 mAh g^{-1}) and S/C (702 mAh g^{-1}). Significantly, after 100 discharge–charge cycles, the cp(S-PMAT)/C cathode retained 99.0 % of its specific capacity (1074 mAh g^{-1}). This corresponds to a diminishment of only 0.013 % per cycle, which is an order of magnitude lower than those for S&PMAT/C (0.103 %) and S/C (0.155 %). The remarkable performance of the cp(S-PMAT)/C electrode most likely arises from its highly crosslinked structure and high electrical conductivity.

At lower current rates, the S/C electrode showed two discharge voltage plateaus at approximately 2.45 and 2.00 V (vs. Li$^+$/Li) and two charge voltage plateaus at approximately 2.25 and 2.48 V (Figure S8 a). These observations coincide with the cyclic voltammetry (CV) results, in which the S/C electrode exhibited two cathodic peaks at 2.41 and 1.93 V and anodic peaks at 2.42 and 2.50 V (Figure S8 b). On the basis of the previously reported mechanisms,[24] the appearance of voltage plateaus is attributed to the reduction/oxidation of sulfur during the discharge/charge processes, the discharge voltage plateau at approximately 2.45 V is ascribed to the reduction of S_8 to high-order Li_2S_x ($x = 4$ to 8), and the plateau at approximately 2.00 V is caused by the further reduction of the high-order polysulfides Li_2S_x to Li_2S_2 and finally to Li_2S. Accordingly, the two voltage plateaus at approximately 2.25 and 2.48 V in the charge profiles arise from the oxidation of Li_2S to Li_2S_x and then S_8, respectively. In contrast, for the voltage profiles depicted in Figure 4 e, the cp(S-PMAT) electrode showed two plateaus at approximately 2.18 and 1.93 V during discharge but only one at approximately 2.38 V in the charge profile (Figure 4 e). In the corresponding cyclic voltammetric measurements (Figure S8 b), cp(S-PMAT) exhibited a quasisingle peak at approximately 2.33 V in the anodic scan and two peaks at 2.20 and 1.88 V in the cathodic scan. The distinct differences in the charge profiles and anodic CV scans for the cp(S-PMAT)/C electrode compared with those of S/C indicate that the final discharge product Li_2S was eventually oxidized and reassembled into the crosslinked sulfur side chains of PMAT rather than forming physically adsorbed S_8 in the charge process. Such a stable crosslinked nanostructure is highly desired for the implementation of long-life Li–S batteries.

As shown in Figure 4 f, the cp(S-PMAT) electrode shows reversible discharge–charge capacities of 1240 mAh g^{-1} at 0.1 C, 1085 mAh g^{-1} at 0.2 C, 976 mAh g^{-1} at 0.5 C, 880 mAh g^{-1} at 1 C, 780 mAh g^{-1} at 2 C, and 600 mAh g^{-1} at 5 C, which are much higher than those of the S&PMAT and S/C electrodes. Note that the rate performance of the cp(S-PMAT)/C electrode is even better than (or at least comparable to) the leading results for relevant polymer cathodes reported recently (Table S1). Moreover, the discharge voltages of cp(S-PMAT)/C remained almost invariant within the current range 0.1 to 2 C, whereas that of the S/C electrode started to change markedly at a much lower rate of 0.5 C (Figure S8 a). Again, this excellent rate performance may be ascribed to the conducting and highly crosslinked nanostructures of cp(S-PMAT).

To study the electrochemical performance of the polymer cathodes, discharge–charge cycling experiments were conducted with a series of cp(S-PMAT)/C electrodes at different sulfur loadings. As shown in Figure 5 a, the cp(S-PMAT)/C electrode at

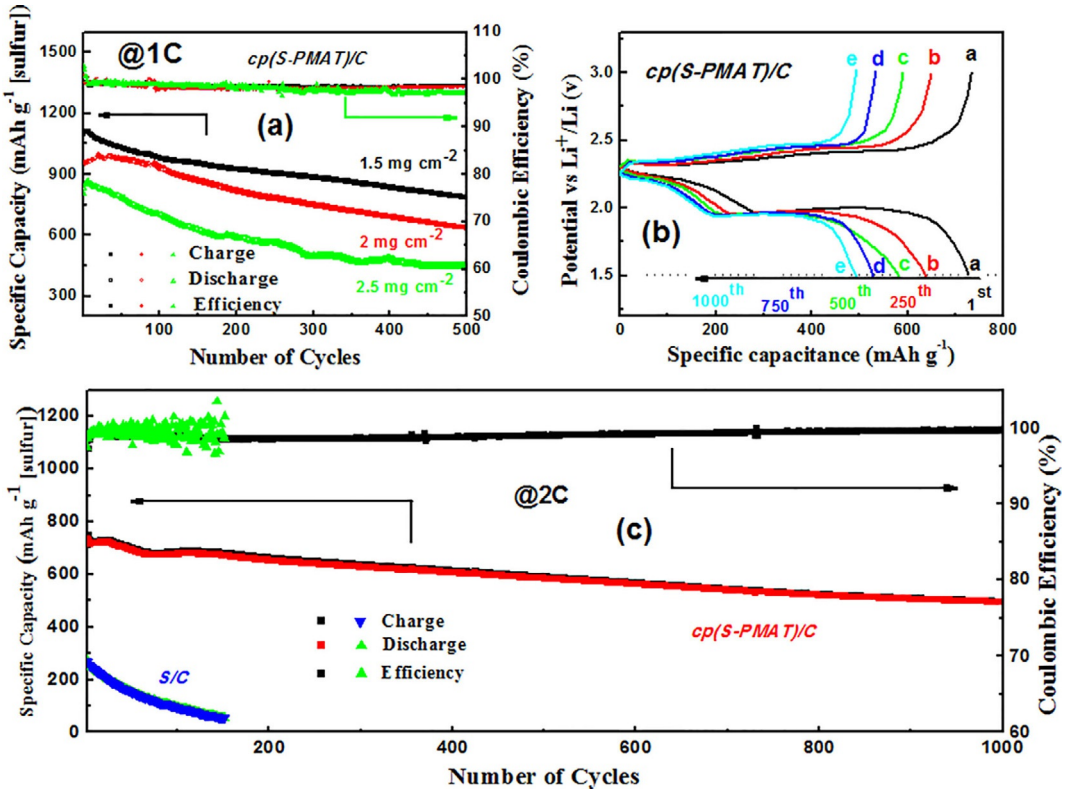

Figure 5. (a) Cycling performances of cp(S-PMAT)/C cathodes at different sulfur loadings. (b) Discharge–charge profiles of the cp(S-PMAT)/C cathode at 1 C at an active sulfur loading of 1.5 mg cm^{-2}. (c) Cycling performance and coulombic efficiency of cp(S-PMAT)/C cathodes at 2 C.

1 C exhibited a clear decrease of the initial discharge capacity with increasing sulfur loading from 1085 mAh g^{-1} at a sulfur loading of 1.5 mg cm^{-2} to 968 mAh g^{-1} at 2.0 mg cm^{-2} and 853 mAh g^{-1} at 2.5 mg cm^{-2}. This may be accounted for by a reduced utilization of sulfur. A similar trend was observed in the cycling stability. For example, after 500 discharge–charge cycles, the discharge capacity decreased by 28.7% at a sulfur loading of 1.5 mg cm^{-2}, 33.9% at 2.0 mg cm^{-2}, and 46.1% at 2.5 mg cm^{-2}. This is because the thickness of the cp(S-PMAT) film increases as the sulfur loading increases and impedes the diffusion of Li ions, which leads to incomplete discharge–charge processes. Note that incomplete discharge–charge processes will facilitate the formation of polysulfide intermediates, which can be dissolved readily into the electrolyte. Consequently, the content of active sulfur in the thick film decreases quickly, and this leads to rapid capacity degradation.

The long-term cycling performance of the cp(S-PMAT)/C cathode was then evaluated at a high rate of 2 C. As shown in Figure 5 b, although the capacity of the cp(S-PMAT)/C cathode declined gradually with increasing cycle number, the discharge voltage remained virtually unchanged. From Figure 5 c, it can be seen that the specific capacity of the S/C electrode decreased rapidly from the initial 272 mAh g^{-1} to 56 mAh g^{-1} after only 150 cycles. In sharp contrast, the cp(S-PMAT)/C electrode delivered a remarkable initial capacity of 739 mAh g^{-1}, and the retained capacity of 495 mAh g^{-1} even after 1000 deep discharge–charge cycles corresponds to a capacity retention of 66.9% and a fading rate of only 0.040% per cycle. Moreover, the coulombic efficiency for the cp(S-PMAT)/C electrode remained close to 100% during the 1000 discharge–charge cycles. Even after normalization to the total mass of the electrode, the cp(S-PMAT)/C cathode still exhibited a high capacity of 500 mAh g^{-1} (Figure S9), which is much higher than that of the S/C electrode.[17a,26] The dramatically enhanced capacity and cycling stability of cp(S-PMAT)/C are attributed to the formation of a highly crosslinked sulfur-rich conducting copolymer.

The distinct difference in capacitive performance is illustrated further by light-emitting diodes (LEDs) powered by coin-type Li–S batteries with different cathode materials. As shown in Figure S10, the battery with a S/C cathode was almost out of power after only 2 h of operation, whereas the battery with a cp(S-PMAT)/C cathode was able to power the LED for 3 h without a significant reduction in brightness. This observation clearly signifies that cp(S-PMAT)/C possesses a significantly higher energy storage capacity than that of the S/C electrode.

The structural integrities of the cathode materials during the discharge–charge cycles were evaluated by SEM measurements. As depicted in Figure 6 a, dense nanoparticles can be seen on the S/C electrode surface; after 150 discharge–charge cycles at 2 C, some large cavities with diameters ranging from submicron to several microns appeared and could be ascribed to the dissolution of sulfur in the form of polysulfides. For the cp(S-PMAT)/C electrode, the surface before cycling consists of many tiny holes/voids that would lead to the tolerance of volume expansion (Figures 6 c and S11), and this morphology

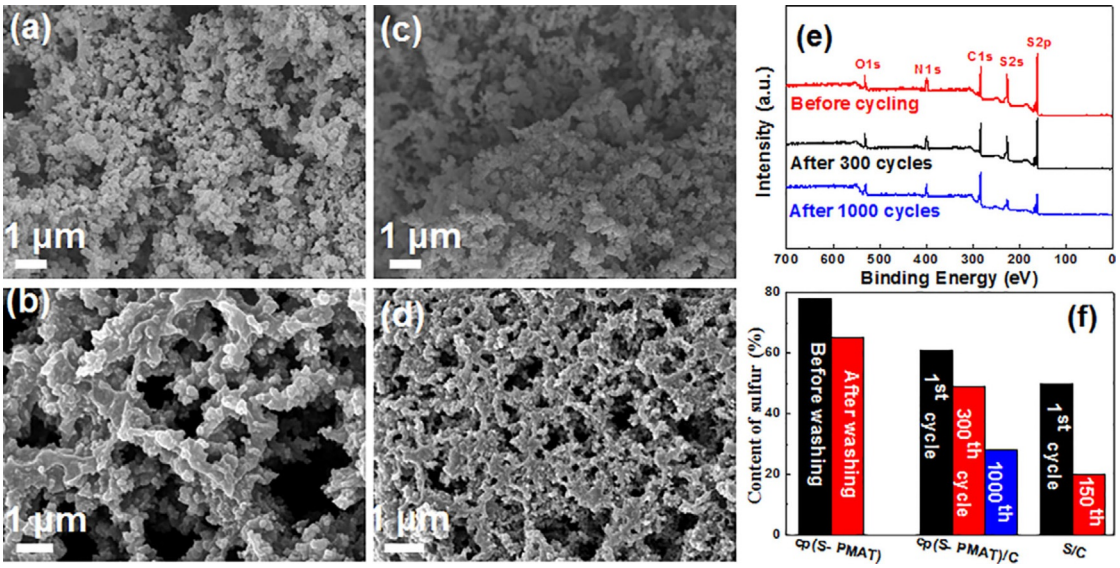

Figure 6. SEM images of the S/C electrode (a) before and (b) after 150 discharge–charge cycles at 2 C and the cp(S-PMAT)/C electrode (c) before and (d) after 1000 discharge–charge cycles at 2 C. (e) XPS survey spectra of the cp(S-PMAT)/C electrode after different discharge–charge cycles at 2 C. (f) Sulfur contents of the samples after different treatments.

remained largely unchanged even after 1000 discharge–charge cycles at 2 C (Figure 6 d), but the cavities were significantly smaller. This suggests that the cycling stability of sulfur in cp(S-PMAT)/C was enhanced dramatically compared with that of the S/C electrode owing to the covalent bonding with the thiol groups of PMAT.

The electrode sulfur content was also monitored quantitatively through XPS measurements. As shown in Figure S4 b, the relative intensities of the S 2s and S 2p peaks for S/C decreased drastically owing to the dissolution of a large quantity of polysulfides into the electrolyte. The decline occurred at a much slower rate for cp(S-PMAT) (Figure 6 e) from 61 wt% before cycling to 49 wt% after 300 cycles and 30 wt% after 1000 cycles (Figure 6 f). Consistent results were obtained through EDS (Figure S12), FTIR spectroscopy, and Raman spectroscopy (Figure S13), through which a vibrational band was observed at $\tilde{\nu}=780\ cm^{-1}$ for the stretching vibration of the C–S bond,[17a,27] and another at $\tilde{\nu}=1000\ cm^{-1}$ was attributed to the S–S stretching vibration.[27] No apparent variations were observed with the cp(S-PMAT) electrode even after 1000 discharge–charge cycles at 2 C; therefore, cp(S-PMAT) was structurally robust. Taken together, these observations show clearly that the copolymerization of sulfur with PMAT to form covalent bonds between sulfur and the thiol groups of PMAT represents an effective strategy for the chemical confinement of active sulfur and leads to a dramatic enhancement of the rate performance and cycling stability of sulfur-containing cathodes in Li–S batteries.

Conclusion

Organosulfur cathodes were synthesized by a facile and scalable strategy through the direct copolymerization of sulfur with preformed poly(*m*-aminothiophenol) (PMAT) through inverse vulcanization. The thus-synthesized cp(S-PMAT) copolymer contained approximately 80 wt% of sulfur, which was crosslinked with the conducting polymer and exhibited a crystalline phase. Electrochemical measurements showed the excellent rate performance of the cp(S-PMAT) cathode, which has capacities of 880 mAh g^{-1} at 1 C, 780 mAh g^{-1} at 2 C, and 600 mAh g^{-1} at 5 C. Notably, the cp(S-PMAT) cathode retained a high capacity of 495 mAh g^{-1} after 1000 cycles with an unprecedented capacity retention rate of over 66.9% at a high charge–discharge current of 2 C, which corresponds to a rate diminishment of only 0.040% per cycle. This may be ascribed to the conductive and stable crosslinked network structure of the copolymer cathode, which not only exhibited effective pathways for electron and ion transports but also confined sulfur strongly through abundant chemical bonds with the PMAT backbone. These results indicate that copolymerization is a facile method for the effective chemical confinement of polysulfides to improve the performances of Li–S batteries.

Experimental Section

Synthesis of PMAT

In a typical reaction, *m*-aminothiophenol (3 g) was dispersed in a 1 M HCl aqueous solution under magnetic stirring in an Ar-filled round-bottomed flask. The temperature of the solution was maintained at 0 °C with an ice bath. A 1 M ammonium persulfate (APS) aqueous solution (30 mL) was added slowly into the above solution. The color of the mixture changed gradually from gray to light brown to dark brown and finally green, which signified the polymerization of *m*-aminothiophenol to PMAT. The reaction proceeded overnight in an ice bath. The solid product was collected, washed several times with deionized (DI) water, and dried at 30 °C in a vacuum oven to afford the PMAT product.

Preparation of cp(S-PMAT)

The PMAT was mixed with sulfur at a PMAT/sulfur mass ratio of 1:6. The mixture was heated at 150 °C for 1 h in an argon atmosphere to impregnate the molten sulfur into the PMAT and then heated further at 170 °C for 8 h to initiate the ring-opening polymerization of sulfur with PMAT to form the highly crosslinked cp(S-PMAT) copolymer.

Materials characterization

The SEM measurements were conducted with a Hitachi S-4800 field-emission scanning electron microscope (FESEM). The TEM measurements were conducted with a JEOL JEM-2100 transmission electron microscope operated at an accelerating voltage of 200 kV. The XRD profiles were obtained with a Bruker D8 instrument with CuK_α radiation. The FTIR spectra were recorded with a Nicolet 6700 FTIR spectrometer in transmittance mode. The UV/Vis absorption spectroscopy measurements were performed with a UV-2600 spectrophotometer. The Raman spectra were acquired with a Lab RAM HR Evolution Raman spectrometer. The XPS measurements were performed with a Phi X-tool XPS instrument. The TGA was performed with a Mettler instrument under a N_2 atmosphere at a ramping rate of 10 °C min^{-1}. For the electrical conductivity measurements, powder materials were compressed at a pressure of 40 MPa with a tablet-compression machine to form circular sheets with the same diameter. The electrical conductivities were measured with a Keithley 2636B source-meter by a two-probe method.

To ensure that the un-crosslinked sulfur was removed completely by CS_2 washing, the sulfur-rich composites dispersed in CS_2 were subjected to ultrasonic agitation in a water bath set at 25 °C for approximately 1 h and then dried for subsequent XRD, XPS, and EDS measurements.

Coin-cell fabrication and battery tests

In brief, polyvinylidene fluoride (PVDF), which served as a binder, was dissolved in *N*-methyl-2-pyrrolidene (NMP) under vigorous magnetic stirring. The active material cp(S-PMAT) and conductive carbon black (Super P, Taiyuan Liyuan Li-ion Battery Technology co., Ltd.) were added into the PVDF solution to form a homogenous slurry at a cp(S-PMAT)/PVDF/conductive carbon black mass ratio of 80:10:10. Subsequently, the slurry was deposited on aluminium foil, which was used as a current collector, by the doctor-blade method and then dried at 45 °C for 24 h in a vacuum oven. The thus-prepared cathode foil was pressed and cut into circular sheets with a diameter of 12 mm. The mass loading of active sulfur was varied from 1.5 to 2.0 and 2.5 mg cm^{-2} depending on the thickness of the coating layer. The CR2032-type coin cells were assembled in an Ar-filled glovebox with oxygen and moisture contents of less than 0.1 ppm. The cell comprised a cp(S-PMAT) positive electrode, a Celgard 2400 diaphragm separator, lithium foil as the reference/counter electrode, and a mixed solution of 1,3-dioxolane and 1,2-dimethoxyethane (1:1 v/v) containing 1 M lithium bis(-trifluoromethanesulfonyl)imide (LiTFSI) and 0.1 M $LiNO_3$ as the electrolyte. For comparison, coin cells with a mixture of PMAT and S as the cathode (S&PMAT) were prepared in a similar manner at the same loading of active sulfur. In addition, conventional sulfur cathodes were also prepared at a sulfur/conductive carbon black/PVDF mass ratio of 50:40:10 (also the same mass loading of active sulfur).

Galvanostatic discharge–charge measurements of the as-fabricated cells were performed by potential cycling between 1.5 and 3.0 V (vs. Li/Li^+) at different current rates with a button-cell testing system (LANHE CT2001A, 5 V, 20 mA). The cyclic voltammograms were recorded within the potential range 1.5 to 3.0 V at various scan rates. The EIS studies were performed in the charge state between frequencies of 100 kHz and 10 mHz at an alternating current (AC) amplitude of 5 mV.

Acknowledgements

This work was supported by the National Natural Science Foundation of China (NSFC 21528301 and 51402111), Guangdong Innovative and Entrepreneurial Research Team Program (2014ZT05N200), and the Fundamental Research Funds for the Central Universities (SCUT Grant No. 2153860).

Keywords: conducting materials · copolymerization · electrochemistry · lithium · sulfur

[1] a) L. Borchardt, M. Oschatz, S. Kaskel, *Chem. Eur. J.* **2016**, *22*, 7324 – 7351; b) M. A. Pope, I. A. Aksay, *Adv. Energy Mater.* **2015**, *5*, 1500124.
[2] H. Cheng, S. Wang, *J. Mater. Chem. A* **2014**, *2*, 13783 – 13794.
[3] a) V. Etacheri, R. Elazari, G. Salitra, D. Aurbach, *Energy Environ. Sci.* **2011**, *4*, 3243 – 3262; b) D. Zheng, X. Q. Yang, D. Qu, *ChemSusChem* **2016**, *9*, 2348 – 2350.
[4] D. Bresser, S. Passerini, B. Scrosati, *Chem. Commun.* **2013**, *49*, 10545 – 10562.
[5] L. Wang, D. Wang, F. Zhang, J. Jin, *Nano Lett.* **2013**, *13*, 4206 – 4211.
[6] Y. Xiang, J. Li, J. Lei, D. Liu, Z. Xie, D. Qu, K. Li, T. Deng, H. Tang, *ChemSusChem* **2016**, *9*, 3023 – 3039.
[7] J. Wang, J. Yang, C. Wan, K. Du, J. Xie, N. Xu, *Adv. Funct. Mater.* **2003**, *13*, 487 – 492.
[8] a) J. Zhou, X. Yu, X. Fan, X. Wang, H. Li, Y. Zhang, W. Li, J. Zheng, B. Wang, X. Li, *J. Mater. Chem. A* **2015**, *3*, 8272 – 8275; b) H. Yang, S. J. Bradley, A. Chan, G. I. Waterhouse, T. Nann, P. E. Kruger, S. G. Telfer, *J. Am. Chem. Soc.* **2016**, *138*, 11872 – 11881.
[9] a) G. Li, J. Sun, W. Hou, S. Jiang, Y. Huang, J. Geng, *Nat. Commun.* **2016**, *7*, 10601; b) J. Song, T. Xu, M. L. Gordin, P. Zhu, D. Lv, Y. B. Jiang, Y. Chen, Y. Duan, D. Wang, *Adv. Funct. Mater.* **2014**, *24*, 1243 – 1250; c) C. H. Chang, S. H. Chung, A. Manthiram, *Small* **2016**, *12*, 174 – 179; d) S. H. Chung, P. Han, R. Singhal, V. Kalra, A. Manthiram, *Adv. Energy Mater.* **2015**, *5*, 1500738; e) R. Singhal, S. H. Chung, A. Manthiram, V. Kalra, *J. Mater. Chem. A* **2015**, *3*, 4530 – 4538; f) R. Elazari, G. Salitra, A. Garsuch, A. Panchenko, D. Aurbach, *Adv. Mater.* **2011**, *23*, 5641 – 5644; g) M. Behzadirad, O. Lavrova, T. Busani, *J. Mater. Chem. A* **2016**, *4*, 7830 – 7840; h) C. Tang, B. Q. Li, Q. Zhang, L. Zhu, H. F. Wang, J. L. Shi, F. Wei, *Adv. Funct. Mater.* **2016**, *26*, 577 – 585.
[10] S. H. Chung, C. H. Chang, A. Manthiram, *Energy Environ. Sci.* **2016**, *9*, 3188 – 3200.
[11] Z. W. Seh, W. Li, J. J. Cha, G. Zheng, Y. Yang, M. T. McDowell, P. C. Hsu, Y. Cui, *Nat. Commun.* **2013**, *4*, 1331.
[12] a) L. Qie, A. Manthiram, *Adv. Mater.* **2015**, *27*, 1694 – 1700; b) N. Osada, C. B. Bucur, H. Aso, J. Muldoon, *Energy Environ. Sci.* **2016**, *9*, 1668 – 1673.
[13] H. Wang, W. Zhang, H. Liu, Z. Guo, *Angew. Chem. Int. Ed.* **2016**, *55*, 3992 – 3996; *Angew. Chem.* **2016**, *128*, 4060 – 4064.
[14] R. Chen, T. Zhao, J. Lu, F. Wu, L. Li, J. Chen, G. Tan, Y. Ye, K. Amine, *Nano. Lett.* **2013**, *13*, 4642 – 4649.
[15] Q. Zhang, X. B. Cheng, J. Q. Huang, H. J. Peng, F. Wei, *Carbon* **2015**, *81*, 850 – 852.
[16] Z. Li, J. Zhang, B. Guan, D. Wang, L. M. Liu, X. W. Lou, *Nat. Commun.* **2016**, *7*, 13065.
[17] a) S. N. Talapaneni, T. H. Hwang, S. H. Je, O. Buyukcakir, J. W. Choi, *Angew. Chem. Int. Ed.* **2016**, *55*, 3106 – 3111; *Angew. Chem.* **2016**, *128*, 3158 – 3163; b) W. J. Chung, J. J. Griebel, E. T. Kim, H. Yoon, A. G. Simmonds, H. J. Ji, P. T. Dirlam, R. S. Glass, J. J. Wie, N. A. Nguyen, B. W. Gur-

alnick, J. Park, A. Somogyi, P. Theato, M. E. Mackay, Y. E. Sung, K. Char, J. Pyun, *Nat. Chem.* **2013**, *5*, 518 – 524; c) S. Diez, A. Hoefling, P. Theato, W. Pauer, *Polymer* **2017**, *9*, 59 – 66; d) T. Tsuda, A. Takeda, *Chem. Commun.* **1996**, 1317 – 1318; e) Y. Ding, A. S. Hay, *J. Polym. Sci. Part A* **1997**, *35*, 2961 – 2968; f) H. Kim, J. Lee, H. Ahn, O. Kim, M. J. Park, *Nat. Commun.* **2015**, *6*, 7278; g) Y. Fu, A. Manthiram, *Chem. Mater.* **2012**, *24*, 3081 – 3087.

[18] a) B. Oschmann, J. Park, C. Kim, K. Char, Y. E. Sung, R. Zentel, *Chem. Mater.* **2015**, *27*, 7011 – 7017; b) B. C. Yu, J. W. Jung, K. Park, J. B. Goodenough, *Energy Environ. Sci.* **2017**, 10, 86 – 90; c) A. Chang, Q. Wu, X. Du, S. Chen, J. Shen, Q. Song, J. Xie, W. Wu, *Chem. Commun.* **2016**, *52*, 4525 – 2528; d) S. Zeng, L. Li, D. Zhao, J. Liu, W. Niu, N. Wang, S. Chen, *J. Phys. Chem. C* **2017**, *121*, 2495 – 2503.

[19] Y. Cui, Y. Fu, *ACS Appl. Mater. Interfaces* **2015**, *7*, 20369 – 20376.

[20] a) N. Xu, T. Qian, X. Liu, J. Liu, Y. Chen, C. Yan, *Nano Lett.* **2017**, *17*, 538 – 543; b) B. Li, S. Li, J. Xu, S. Yang, *Energy Environ. Sci.* **2016**, *9*, 2025 – 2030.

[21] B. Ding, Z. Chang, G. Xu, P. Nie, J. Wang, J. Pan, H. Dou, X. Zhang, *ACS Appl. Mater. Interfaces* **2015**, *7*, 11165 – 11171.

[22] a) C. Zu, A. Manthiram, *Adv. Energy Mater.* **2013**, *3*, 1008 – 1012; b) T. Ramanathan, F. T. Fisher, R. S. Ruoff, L. C. Brinson, *Chem. Mater.* **2005**, *17*, 1290 – 1295.

[23] a) X. Peng, K. Huo, J. Fu, X. Zhang, B. Gao, P. K. Chu, *Chem. Commun.* **2013**, *49*, 10172 – 10174; b) J. Chen, Z. Xia, H. Li, Q. Li, Y. Zhang, *Electrochim. Acta* **2015**, *166*, 174 – 182.

[24] C. O. Baker, X. Huang, W. Nelson, R. B. Kaner, *Chem. Soc. Rev.* **2017**, *46*, 1510 – 1525.

[25] Z. Wang, Y. Dong, H. Li, Z. Zhao, H. B. Wu, C. Hao, S. Liu, J. Qiu, X. W. Lou, *Nat. Commun.* **2014**, *5*, 5002.

[26] a) M. R. Kaiser, X. Liang, H. K. Liu, S. X. Dou, J. Z. Wang, *Carbon* **2016**, *103*, 163 – 171; b) S. Li, T. Mou, G. Ren, J. Warzywoda, B. Wang, Z. Fan, *ACS Energy Lett.* **2016**, *1*, 481 – 489.

[27] W. Li, M. Zhou, H. Li, K. Wang, S. Cheng, K. Jiang, *Energy Environ. Sci.* **2015**, *8*, 2916 – 2921.

Manuscript received: May 24, 2017
Revised manuscript received: June 22, 2017
Accepted manuscript online: July 24, 2017
Version of record online: August 21, 2017